SANDIA REPORT

SAND97-1174 • UC-705
Unlimited Release
Printed May 1997

Spherical Cavity-Expansion Forcing Function in PRONTO 3D for Application to Penetration Problems

Thomas L. Warren, Mazen R. Tabbara

Approved for public release; distribution is unlimited.

MASTER

RECEIVED

JUN 0 1 1997

OSTI

Sandia National Laboratories

DISTRIBUTION OF THIS DOCUMENT IS UNLIMITED

HH

DISCLAIMER

Portions of this document may be illegible in electronic image products. Images are produced from the best available original document.

Spherical Cavity-Expansion Forcing Function in PRONTO 3D for Application to Penetration Problems

Thomas L. Warren

Advanced Concepts and Penetration Technology Department

Mazen R. Tabbara

Material and Structural Mechanics Department

Sandia National Laboratories

P.O. Box 5800

Albuquerque, New Mexico 87185-0303

Abstract

In certain penetration events the primary mode of deformation of the target can be approximated by known analytical expressions. In the context of an analysis code, this approximation eliminates the need for modeling the target as well as the need for a contact algorithm. This technique substantially reduces execution time. In this spirit, a forcing function which is derived from a spherical-cavity expansion analysis has been implemented in PRONTO 3D. This implementation is capable of computing the structural and component responses of a projectile due to three dimensional penetration events. Sample problems demonstrate good agreement with experimental and analytical results.

3

Acknowledgments

Table of Contents

Figures

Nomenclature

a	cavity radius
b_1	first bounding coordinate
b_2	second bounding coordinate
c_1	constant term nodal pressure coefficient
c_2	linear term nodal pressure coefficient
c_3	quadratic term nodal pressure coefficient
f_c'	unconfined compressive strength of concrete
m	mass of the projectile
$\vec{n}$	unit outward normal vector
p_I	pressure at node I
$\vec{V}_I$	velocity vector at node I
ϑ	target particle velocity at the nose-target interface
A	constant term dimensionless fitting coefficient
B	linear term dimensionless fitting coefficient
C	quadratic term dimensionless fitting coefficient
E	Young's modulus
I	integer variable with range 1 to 4 corresponding to element side nodes
N	geometric parameter
P	depth of penetration
S	empirical dimensionless constant
V_s	striking velocity of the projectile
Y	quasi-static yield strength
ν	Poisson's ratio
ρ_o	density of the undeformed target material
ρ_p	density of the undeformed projectile material
σ_r	radial stress at the cavity surface
$\overline{\sigma}_r$	average radial stress at the cavity surface
ψ	caliber-radius-head (CRH)

Spherical Cavity Expansion Forcing Function in PRONTO 3D for Application to Penetration

Introduction

Computational modeling of penetration and perforation remains to be an active field of research. A literature search on this topic reveals numerous recent publications that propose new methods or improve existing ones. There has been considerable effort and progress in the development of various codes (based on different representations of the conservation laws for a continuum: Lagrangian, Eulerian, Arbitrary Lagrangian-Eulerian, etc.) that serve as powerful and versatile computational tools which are routinely used to solve complex problems. However, at present, the time required to complete a single penetration run is still excessive and prohibits any prospect for streamlining the penetration analysis for use in an overall design tool that would permit numerous simulations.

In cases where the deformation mode of the target can be captured (to first order) by a known analytical model and where the primary interest is in the structural response of the projectile, the penetration analysis can then be reduced to modeling the projectile by itself. The target is replaced by a known forcing function that approximates its resistance. This eliminates the need to model the target and furthermore eliminates the need for a contact algorithm, which leads to substantial savings in execution time.

Forrestal et al. (1988) recognized that the resistance produced by an aluminum target could be approximated by a dynamic cavity-expansion analysis. They developed closed-form expressions for the depth of penetration of rigid projectiles with different nose shapes and demonstrated good agreement with experimental results. The same concept is applied here, but in the context of a three dimensional finite element code. A forcing function based on the dynamic expansion of a spherical cavity is implemented in the Sandia developed explicit dynamic finite element code PRONTO 3D (Taylor and Flanagan, 1987) and can be utilized by analysts who have access to the PRONTO 3D computer code. This implementation is capable of handling a full three dimensional penetration event which

7

includes: oblique impact, nonzero angle of attack, nonlinear deformations of the projectile, response of components internal to the projectile, etc. The accuracy of this method depends on how well the forcing function approximates the actual situation; however, in many cases the spherical cavity expansion (which is derived on the basis of an unbounded medium) does provide a good approximation for events where the free surface effects are minimal. Thus, this implementation is most accurate for cases of deep penetration.

This method has previously been applied with some success using cavity expansion forcing functions with beam elements in the general purpose finite element code ABAQUS implicit (Hibbitt, Karlsson, and Sorensen, Inc., 1989) by Longcope (1991) and Longcope (1996), and using empirical forcing functions with shell elements in ABAQUS implicit by Adley and Moxley (1996), with shell elements in ABAQUS explicit by Duffey and Macek (1997), and also with tetrahedron, brick, and shell elements in EPIC 97 (Johnson et al., 1997).

Analytical Spherical Cavity Expansion

Analytical methods for penetration mechanics began with the work of Bishop, Hill, and Mott (1945). They developed equations for the quasi-static expansions of cylindrical and spherical cavities and used these equations to estimate forces on conical nose punches pushed slowly into metal targets. Goodier (1965) developed a model to predict the penetration depth of rigid spheres launched into metal targets. His penetration model included target inertial effects, so he approximated the target response by results from the dynamic, spherically symmetric, cavity-expansion equations for an incompressible target material derived by Hill (1948) and discussed by Hill (1950) and Hopkins (1960). In more recent work (Forrestal et al., 1988; Forrestal et al., 1991; Forrestal et al., 1995; Forrestal and Tzou, 1996; and Warren and Forrestal, 1997) it has been shown that the radial stress at the cavity surface obtained from spherical cavity-expansion models can be accurately represented by a function of the form

$$\frac{\sigma_r(a)}{Y} = A + B\left(\sqrt{\frac{\rho_o}{Y}}\vartheta\right) + C\left(\sqrt{\frac{\rho_o}{Y}}\vartheta\right)^2 \ , \tag{1}$$

where ϑ is the target particle velocity at the cavity-target interface, a is the cavity radius, Y is the quasi-static yield strength of the target material, ρ_o is the density of the undeformed target material, and A, B, and C are dimensionless fitting coefficients. The expression given in (1) is also consistent with the semi-empirical model developed by Forrestal et al. (1994) for penetration into concrete targets.

Implementation of the Spherical Cavity Expansion Forcing Function in PRONTO 3D

The spherical cavity-expansion forcing function is implemented in PRONTO 3D as a normal traction (or pressure) boundary condition that acts on a prescribed surface. This new option has been added to the PRONTO 3D command language and is invoked with the command line:

CAVIty EXPAntion, side set id AXIS=direction BOUNds=b_1, b_2 COEF=c_1, c_2, c_3

where uppercase letters represent the minimum abbreviation of each word and

side set id	must match a side set on the GENESIS file
direction	X, Y, or Z (default=Z)
b_1, b_2	bounding coordinates along the direction specified in AXIS
c_1, c_2, c_3	constant nodal pressure coefficients.

The command line shown above can be repeated, as needed, in order to represent layers with different parameters.

Four nodal pressures are calculated in PRONTO 3D for each element side (i.e. a side of a hexagonal continuum element or mid-surface of a structural shell element) included in the side set as shown in Fig. 1. These nodal pressures are obtained from

$$p_I = c_1 + c_2\left(\vec{V}_I \bullet \vec{n}\right) + c_3\left(\vec{V}_I \bullet \vec{n}\right)^2 \qquad (I = 1,4) , \qquad (2)$$

where the dot represents a scalar product, $\vec{V_I}$ is the nodal velocity vector, $\vec{n}$ is the outward unit vector normal to the diagonals of the side, and the constant nodal pressure coefficients are related to the dimensionless fitting coefficients in (1) as $c_1 = AY$, $c_2 = B(\rho_o Y)^{1/2}$, and $c_3 = C\rho_o$. The values of p_I are updated during each time increment using the current values of $\vec{V_I}$ and $\vec{n}$. If the scalar product $\left(\vec{V_I} \bullet \vec{n}\right)$ at a node is zero, negative, or if the node lies outside the bounds set by b_1 and b_2 then the pressure is set to zero for that node.

A set of consistent global forces arising from these pressures over an element side are calculated as discussed by Taylor and Flanagan (1987). These forces are accumulated as each element side in the side set is considered.
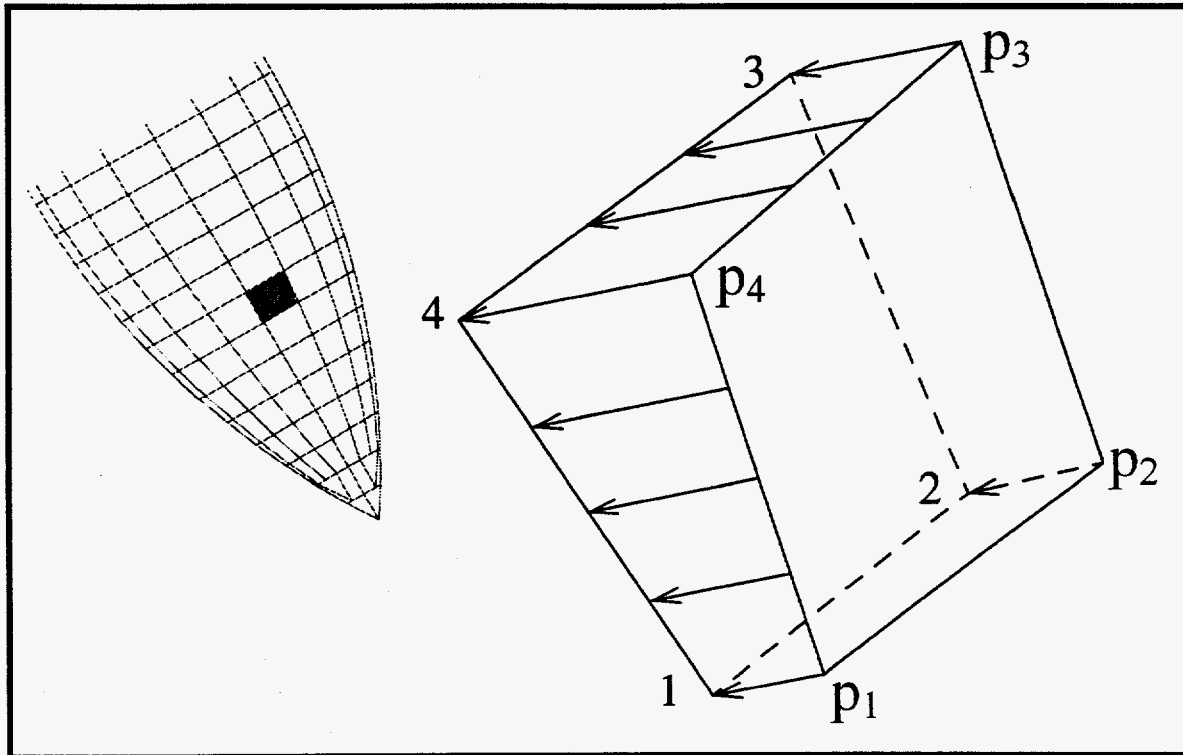

Figure 1. Definition of a pressure boundary condition that acts on an element side.

Numerical Examples

In this section we present example problems of penetration into both aluminum and concrete targets which demonstrate the significant features of the cavity expansion forcing function option in PRONTO 3D. In all of the example problems we only provide the input instructions and not the geometric definitions of the mesh.

Penetration into Aluminum Targets

In these examples we consider the penetration of 6061-T651 aluminum targets by solid spherical-nose, C-300 maraging steel rods launched at striking velocities between 350 and 1200 m/s. These rods have density $\rho_p = 8000 \, \text{kg/m}^3$, shank length L=71.12 mm, nose radius a=3.55 mm, and nominal mass of 0.0235 kg. The target is modeled as a compressible, strain hardening and strain-rate sensitive material for which the undeformed density, quasi-static yield strength, and dimensionless fitting coefficients required for use with (1) are given by Warren and Forrestal (1997) as $\rho_o = 2710 \, \text{kg/m}^3$, Y=276 Mpa, A=5.0394, B=0.9830, and C=0.9402 respectively. The finite element mesh used in the following examples is shown in Fig. 2 and is comprised of 3172 nodes and 2784 elements.

We first compare results obtained by PRONTO 3D with the experimentally verified analytical model given by Warren and Forrestal (1997) in order to validate the cavity expansion forcing function. In the analytical model the projectile is assumed to be rigid; therefore, we use the rigid material model in PRONTO 3D. An example input file for a striking velocity of 960 m/s is shown in Fig. 3. The cavity-expansion command line includes a side set id of 100 which represents the surfaces of the nose and shank (excluding the rear of the projectile). A bounding coordinate, b_1=0 is used to define the free surface and b_2=-10 m to reflect an unbounded medium. Figure 4 shows the depth of penetration at several striking velocities which are in good agreement with the analytical results. A termination time of 350 μs was used for each of the striking velocities, requiring approximately 22 cpu seconds on a CRAY J-90.

11
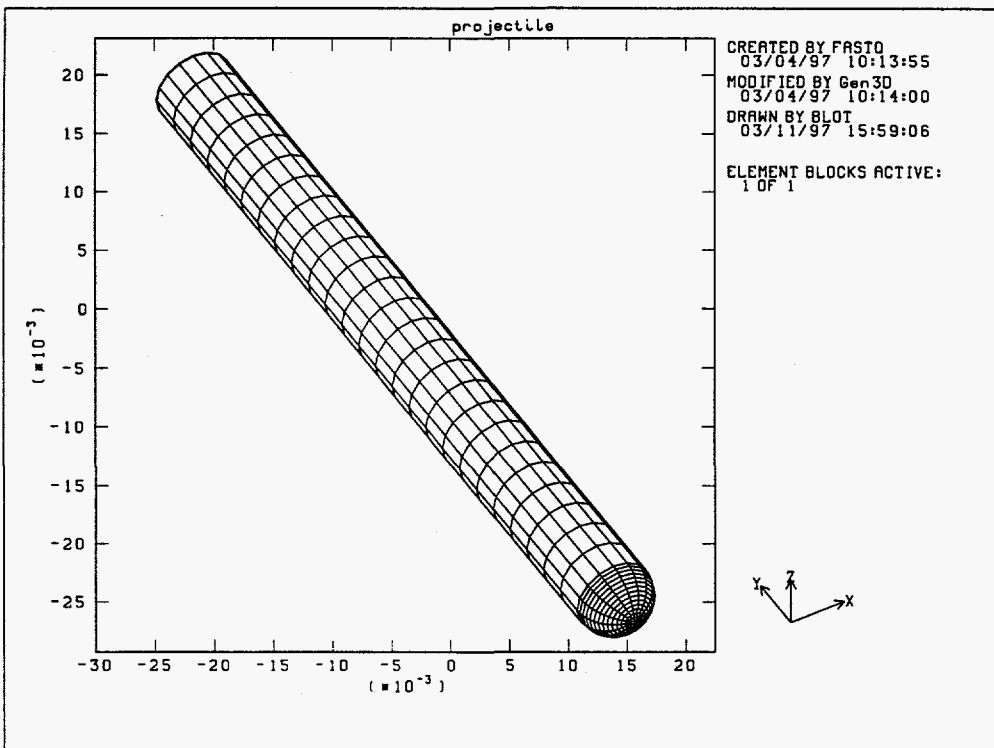
Figure 2. Finite element mesh of the spherical-nose rod.

```
title
penetration into aluminum
material,1,rigid,8000.
contact modulus = 1
end
rigid time step = 3.5e-7
time step scale = 1
bulk viscosity 0,0
initial velocity material,1 0,-960,0
cavity expansion, 100 axis=Y bounds=0,-10 coef=1.39087e9,8.50144e5,2.54794e3
termination time=0.00035
plot time=1.4e-5
history time =7.0e-6
plot nodal= displ,velocity,mass
plot element=eqps,vonmises
plot history coord=0,0,0 vari=velo comp=y name=a
plot history coord=0,0,0 vari=disp comp=y name=a
exit
```

Figure 3. PRONTO 3D input file for the rigid projectile problem.
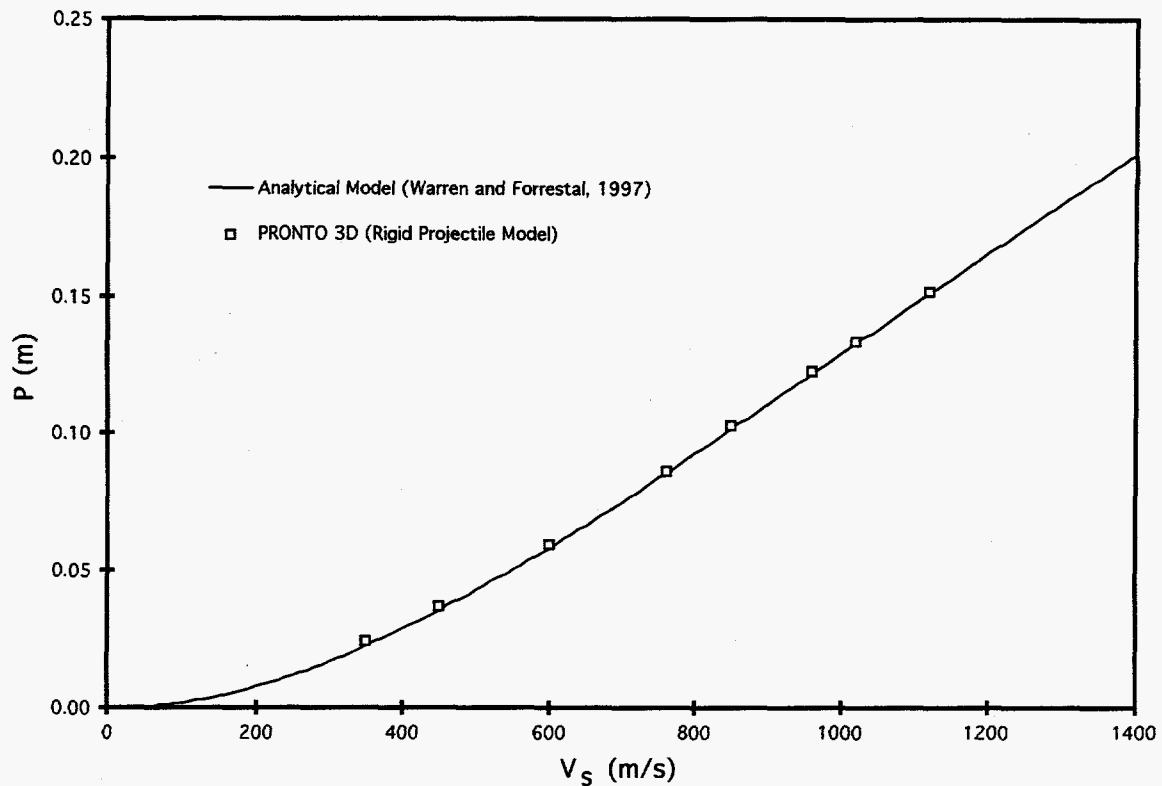
Figure 4. Depth of penetration versus striking velocity for a rigid projectile.

Next, we assume the C-300 maraging steel projectiles to behave as an elastic, linear hardening material and use the elastic-plastic material model in PRONTO 3D. The Young's modulus, yield strength and Poisson's ratio for maraging steel are given by The International Nickel Company, Inc. (1964) as $E = 189$ GPa, $Y = 2.067$ GPa, and $v = 0.3$ respectively. Experimental results obtained by Chait (1972) from compression tests of C-300 maraging steel at room temperature and a strain rate of 3×10^{-4} s^{-1} give a strain hardening modulus of $E' = 177.7$ MPa. An example input file using these parameters is shown in Fig. 5 for a striking velocity of 960 m/s. Depth of penetration results are compared in Fig. 6 with the rigid projectile analytical solution of Warren and Forrestal (1997), and also with experimental data obtained by Forrestal et al. (1988) for C-300 maraging steel and by Forrestal et al. (1991) for T-200 maraging steel which is slightly softer than the C-300 maraging steel. Good agreement is observed between the analytical solution and the PRONTO 3D solution for striking velocities below 700 m/s; however, for higher velocities the projectile deformation reduces the depth of penetration (it should

```
title
penetration into aluminum
material,1,elastic plastic ,8000.
youngs modulus = 189.0e9
poissons ratio = 0.3
yield stress = 2.067e9
hardening modulus = 1.777e8
beta = 1.0
end
time step scale = 1
bulk viscosity 0,0
initial velocity material,1 0,-960,0
cavity expansion, 100 axis=Y bounds=0,-10 coef=1.39087e9,8.50144e5,2.54794e3
termination time=0.00035
plot time=1.4e-5
history time =7.0e-6
plot nodal= displ,velocity,mass
plot element=eqps,vonmises
plot history coord=0,0,0 vari=velo comp=y name=a
plot history coord=0,0,0 vari=disp comp=y name=a
exit
```

Figure 5. PRONTO 3D input file for an elastic-plastic projectile.
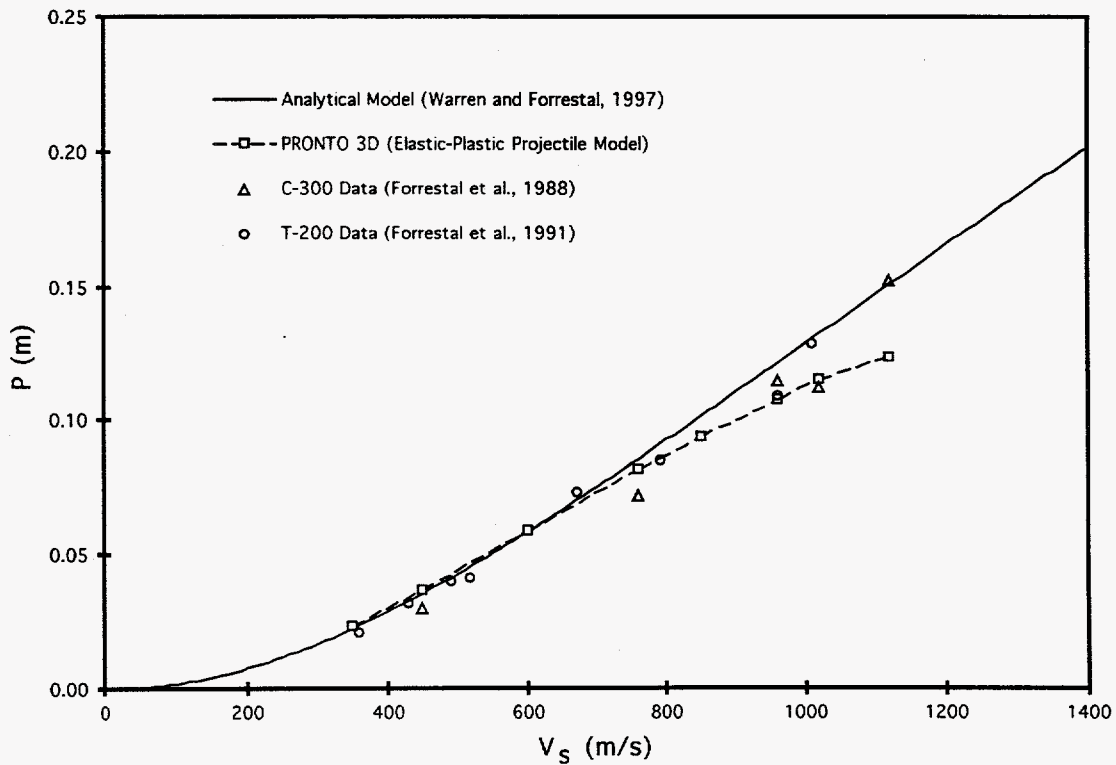
Figure 6. Depth of penetration versus striking velocity for an elastic-plastic projectile.

14

be noted that the depth of penetration would be greater if strain-rate effects had been included in the constitutive model for the penatrator). A sequence of deformed penatrator configurations is shown in Fig. 7 for a striking velocity of V_s=1120 m/s. It is observed that the penetrator bulges slightly early in the penetration event requiring it to open a larger

Figure 7.   Projectile deformation for a striking velocity V_s=1120 m/s at : (a) 0.0 s, (b) 14 μs, (c) 98 μs, and (d) 280 μs.

cavity which reduces the depth of penetration. A termination time of 350 μs was used for each of the striking velocities, requiring approximately 1482 cpu seconds on a CRAY J-90.

As another example we consider the oblique impact of a C-300 maraging steel projectile with a 6061-T651 aluminum target. The input file for a 30 degree oblique impact with a zero angle of attack and a striking velocity of 960 m/s is shown in Fig. 8. A sequence of deformed penatrator configurations for this striking velocity and angle of obliquity is shown in Fig. 9. It is observed that the projectile initially bulges slightly and starts to bend due to the non-symmetric loading. The projectile continues to bend and rotate throughout the penetration event until it finally comes to rest. As in the previous example, a termination time of 350 μs was used requiring approximately 1482 cpu seconds on a CRAY J-90. While we have good agreement between data and predictions for normal impacts, at this time we have no oblique impact data for aluminum targets.

```
title
penetration into aluminum
material,1,elastic plastic ,8000.
youngs modulus = 189.0e9
poissons ratio = 0.3
yield stress = 2.067e9
hardening modulus = 1.777e8
beta = 1.0
end
time step scale = 1
bulk viscosity 0,0
initial velocity material,1 480.0,-831.4,0
cavity expansion, 100 axis=Y bounds=0,-10 coef=1.39087e9,8.50144e5,2.54794e3
termination time=0.00035
plot time=1.4e-5
history time =7.0e-6
plot nodal= displ,velocity,mass
plot element=eqps,vonmises
plot history coord=0,0,0 vari=velo comp=y name=a
plot history coord=0,0,0 vari=disp comp=y name=a
exit
```

Figure 8. PRONTO 3D input file for an oblique impact of 30 degrees.
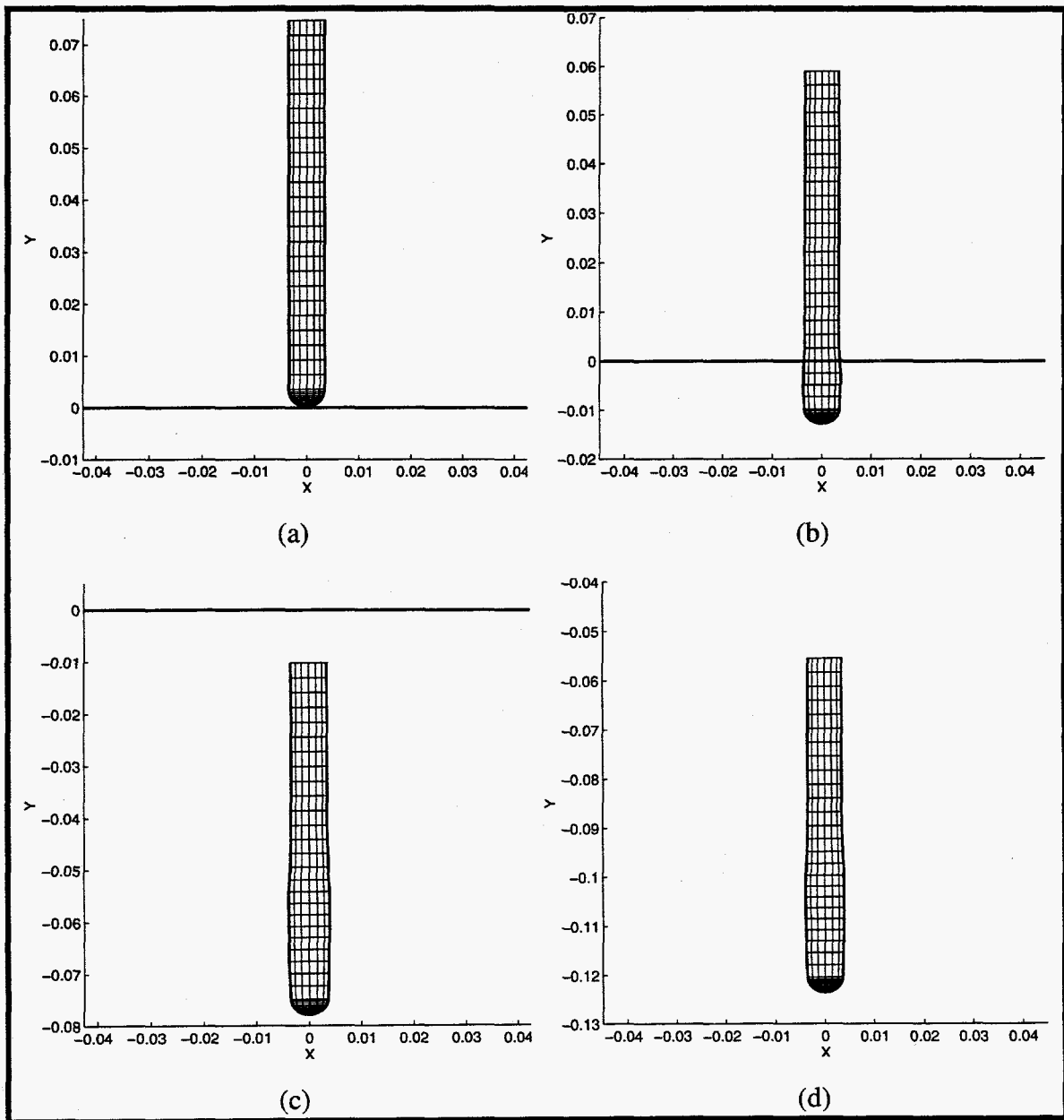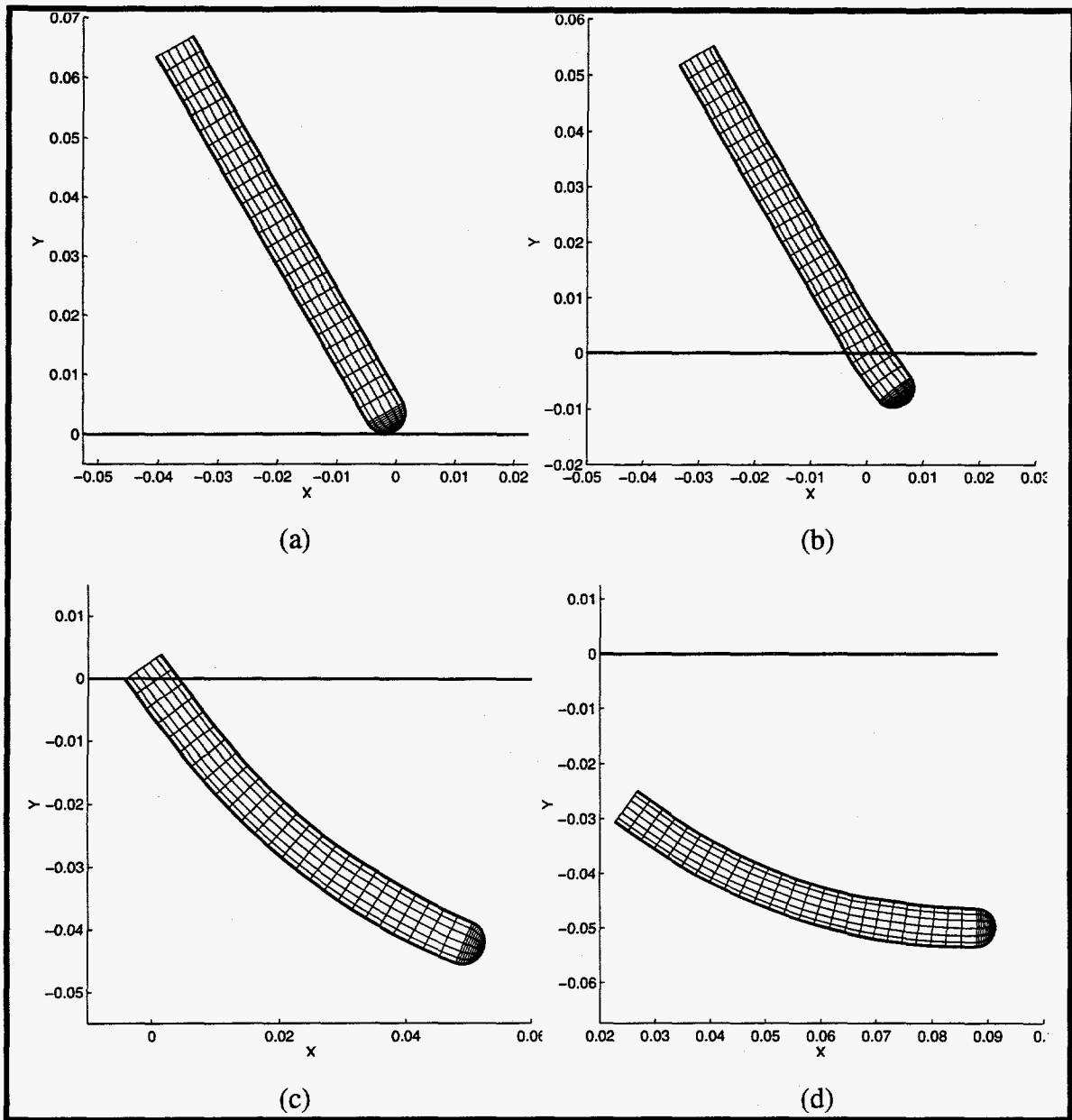
Figure 9.   Projectile deformation for an oblique impact of 30 degrees and a striking
velocity V_s=960 m/s at :(a) 0.0 s, (b) 14 µs, (c) 98 µs,and (d) 252 µs.

Penetration into Concrete Targets

In this example we consider the penetration of 58.4 Mpa (8.5 ksi) concrete targets by solid 3.0 caliber-radius-head (CRH) ogive-nose, 4340 R_c 45 steel rods launched at striking velocities between 400 and 1200 m/s. These rods have density $\rho_p = 7830$ kg/m^3, shank length $L=169.5$ mm, shank diameter $2a=20.3$ mm, nose length $l=33.7$ mm, and nominal mass of 0.478 kg. The coefficients in (1) are obtained using the semi-empirical method developed by Forrestal et al. (1994) for penetration into concrete. The finite element mesh used in this example is shown in Fig. 10 and is comprised of 3197 nodes and 2816 elements.

As discussed by Forrestal et al. (1994) there are two regions in the penetration process of concrete. The first region is a conical cratering region with a depth of approximately two projectile diameters. The second region is the tunneling region which starts at the end of the cratering region and proceeds to the final depth of penetration. For the cratering region we average the expression for the stress (Forrestal et al., 1994) acting on the penetrator over the range $0 \leq y \leq 4a$ which gives

$$\bar{\sigma}_r = \frac{1}{4a} \int_0^{4a} \sigma_r \, dy = \frac{m}{8\pi a^3} \left[V_s^2 - \frac{mV_s^2 - 4\pi a^3 S f_c'}{m + 4\pi a^3 N \rho_o} \right] \, , \tag{3}$$

where m is the mass of the projectile, V_s is the striking velocity, f_c' is the unconfined compressive strength of the target, ρ_o is the density of the undeformed target material, S is an empirical dimensionless constant, and N is a geometric parameter defined by

$$N = \frac{8\psi - 1}{24\psi^2} \, , \tag{4}$$

with ψ being the CRH number. Thus, the value for the constant A in the cratering region is directly obtained from the relation $\bar{\sigma}_r = A f_c'$ (i.e. $B=C=0$), where we take $Y = f_c'$ and for

the given target material $f'_c = 58.4$ MPa, $S=9.037$, and $\rho_o = 2320$ kg/m^3. In the tunneling region $A=S$, $B=0.0$, and $C=1.0$ (Forrestal et al., 1994).

We assume the 4340 R$_c$ 45 steel projectiles to behave as an elastic-plastic power-law hardening material and use the isotropic elastic-plastic power-law hardening material model in PRONTO 3D. The density, Young's modulus, yield strength and Poisson's ratio for 4340 steel projectiles are given by Luk and Piekutowski (1991) as $\rho = 7810$ kg/m^3, $E = 206.8$ GPa, $Y = 1.207$ GPa, and $v = 0.32$ respectively. Curve fitting the data in Luk and Piekutowski (1991) gives a hardening constant of 382 Mpa and hardening exponent of 0.266 which are required for use in the material model. An example input file for a striking velocity of 1162 m/s is shown in Fig. 11. Depth of penetration results are compared in Fig. 12 with the semi-empirical analytical solution of Forrestal et al. (1994), and with experimental data obtained by Frew et al. (1997). Good agreement is observed with both the analytical solution and experimental data. . A termination time of 3000 µs was used for each of the striking velocities, requiring approximately 3785 cpu seconds on a CRAY J-90.
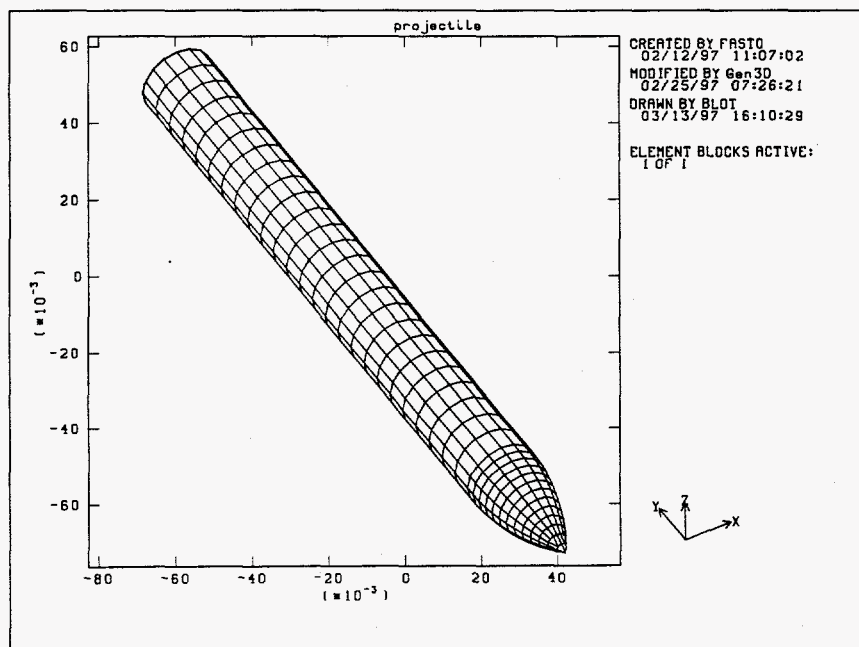
Figure 10. Finite element mesh of the ogive-nose rod.

```
title
penetration into concrete
material,1,ep power hard, 7810.
youngs modulus = 206.8e9
poissons ratio = 0.32
yield stress = 1.207e9
hardening constant = 3.8247155277e8
hardening exponent = 0.2962824
luders strain = 0.0
end
bulk viscosity 0,0
initial velocity material,1 0,-1162.0,0
cavity expansion, 100 axis=Y bounds=0,-0.0406 coef=4.27757e8,0,0.0
cavity expansion, 100 axis=Y bounds=-0.0406,-10 coef=5.277e8,0,2.320e3
termination time=3.0e-3
plot time=1.2e-4
plot element = pressure,eqps,vonmises
plot nodal = displacement,velocity,mass
plot history coord=0,0,0 vari=velo comp=y name=a
plot history coord=0,0,0 vari=disp comp=y name=a
history time=6e-5
exit
```

Figure 11. PRONTO 3D input file for the elastic-plastic power-law hardening projectile.
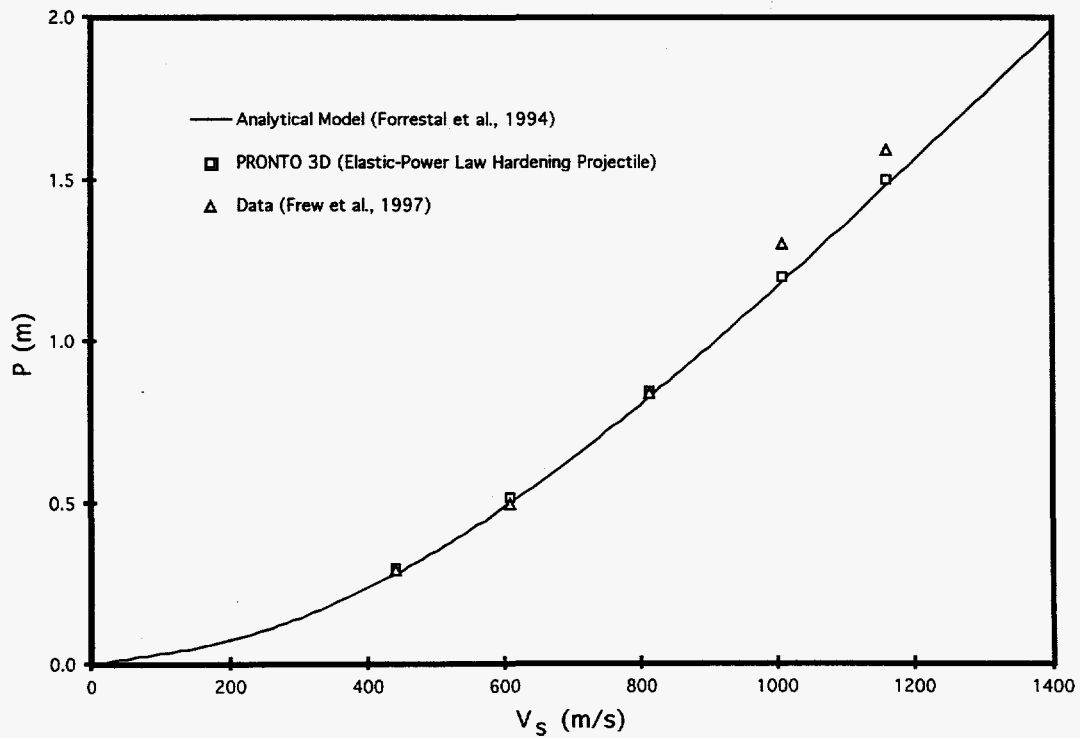
Figure 12. Depth of penetration versus striking velocity for an elastic plastic projectile.

Conclusion

A spherical cavity-expansion forcing function has been implemented into PRONTO 3D. This new capability is intended for analyzing three dimensional penetration events with multi-layered targets. Simulations of normal penetration into aluminum and concrete targets showed good agreement with analytical and experimental results. For the class of problems within the realm of assumptions considered here, this technique is efficient and robust and can be included in a broader software tool utilized for design purposes. Since PRONTO 3D is a Lagrangian code with explicit time integration, good accuracy is expected in computing the structural response of projectiles with nonlinear constitutive models.

References

Adley, M.D., and R.E. Moxley, (1996), PENCURV/ABAQUS: a simply coupled penetration trajectory/structural dynamics model for deformable projectiles impacting complex curvilinear targets, Technical Report SL-96-6, U.S. Army Engineer Waterways Experiment Station, Vicksburg, MS 39180.

Bishop, R.F., R. Hill, and N.F. Mott, (1945), The theory of indentation and hardness, *Proc. Roy. Soc.*, Vol. 57 (3), 147-159.

Chait, R., (1972), Factors influencing the strength differential of high strength steels, *Met. Trans A*, Vol. 3, 365-371.

Duffey, T.A., and R.W. Macek, (1997), Non-normal impact of earth penetrators, *Proceedings of the International Symposium on Penetration and Impact Problems (ICES'97)*, San Jose, Costa Rica.

Forrestal, M.J., K. Okajima, and V.K. Luk, (1988), Penetration of 6061-T651 aluminum targets with rigid long rods, *ASME Journal of Applied Mechanics*, Vol. 55, pp. 755-760.

Forrestal, M.J., N.S. Brar, and V.K. Luk, (1991), Penetration of strain-hardening targets with rigid spherical-nose rods, *ASME Journal of Applied Mechanics*, Vol. 58, pp. 7-10.

Forrestal, M.J. and V.K. Luk, (1991), Penetration into soil targets, *Int. J. Impact Engng.*, Vol. 12, pp.427-444.

Forrestal, M.J., B.S. Altman, J.D. Cargile, and S.J. Hanchak, (1994), An empirical equation for penetration depth of ogive-nose projectiles into concrete targets, *Int. J. Impact Engng.*, Vol. 15, pp.395-405.

Forrestal, M.J., and D.Y. Tzou, E. Askari, and D.B. Longcope, (1995), Penetration into ductile metal targets with rigid spherical-nose rods, *Int. J. Impact Engng.*, Vol. 16, pp.699-710.

Forrestal, M.J., D.Y. Tzou, (1996), A spherical cavity-expansion penetration model for concrete targets, *Int. J. Solids Structures* (accepted).

Frew, D.J., S.J. Hanchak, M.L. Green, and M.J. Forrestal, (1997), Penetration of concrete targets with ogive-nose steel rods, *Int. J. Impact Engng.* (submitted).

Goodier, J.N. (1965), On the mechanics of indentation and cratering in the solid targets of strain-hardening metal by impact of hard and soft spheres, *Proceedings of the 7th Symposium on Hypervelocity Impact III*, 215-259.

Hill, R., (1948), A theory of earth movement near a deep underground explosion, Memo No. 21-48, Armament Research Establishment, Fort Halstead, Kent, UK.

Hill, R., (1950), *The Mathematical Theory of Plasticity*, Oxford University Press, London.

Hopkins, H.G., (1960), Dynamic expansion of spherical cavities in metals, *Progress in Solid Mechanics Vol. 1*, eds. I. Sneddon, and R. Hill, North Holland, New York, 85-164.

Hibbitt, Karlsson, and Sorensen, Inc., (1989), *ABAQUS Users Manual*, Version 4-8, Providence, RI.

The International Nickel Company, Inc., (1964), *18% Nickel Maraging Steels*, New York, NY.

Johnson, G.R., R.A. Stryk, T.J. Holmquist, and S.R. Beissel, (1996), *User Instructions for the 1996 version of the EPIC Code*, Alliant Techsystems Inc., Hopkins, MN.

Johnson, G.R., R.A. Stryk, T.J. Holmquist, and S.R. Beissel, (1997), EPIC 97, software to be released, Alliant Techsystems Inc., Hopkins, MN.

Longcope, D.B., (1991), Coupled bending/lateral load modeling of earth penetrators, SAND90-0789, Sandia National Laboratories, Albuquerque, NM..

Longcope, D.B., (1996), Oblique penetration modeling and correlation with field tests into a soil target, SAND96-2239, Sandia National Laboratories, Albuquerque, NM.

Luk, V.K., and A.J. Piekutowski, (1991), An analytical model on penetration of eroding long rods into metallic targets, *Int. J. Impact Engng.*, Vol. 11, pp.323-340.

Taylor, L.M., and D.P. Flanagan, (1989), PRONTO 3D a three-dimensional transient solid dynamics program, SAND87-1912, Sandia National Laboratories, Albuquerque, NM.

Warren, T.L. and M.J. Forrestal, (1997), Effects of strain hardening and strain-rate sensitivity on the penetration of aluminum targets with spherical-nosed rods, *Int. J. Solids Structures* (submitted).

Distribution:

1 Alliant Techsystems, Inc.
   MS MN11-1614
   Attn: Gordon Johnson
   600 2nd Street, NE
   Hopkins, MN 55343

1 Defense Special Weapons Agency
   HQ/DNA/SPSD
   Attn: Mike Giltrud
   6801 Telegraph Road
   Alexandria, VA 22310-3398

1 Defense Special Weapons Agency
   FC/DSWA
   Attn: George Baladi
   1680 Texas St. SE
   Albuquerque, NM 87117-5669

2 Los Alamos National Laboratory
   Group ESA-EA MS P946
   Attn: Thomas A. Duffey
     Richard W. Macek
   Los Alamos, NM 87545

1 Naval Surface Warfare Center
   NSWCDD, Code G22
   Attn: Walter Hoye
   17320 Dahlgren Road
   Dahlgren, VA 22448-5000

1   Naval Surface Warfare Center
         Indian Head Division
         Attn: John Renzi
         10901 New Hampshire Ave.
         Silver Springs, MD 20903-3090

4   Waterways Experiment Station
         Geomechanics and Explosion Effects
         Attn: Mark Adley
               Rayment E. Moxley
               Rebecca P. Berger
               J. Donald Cargile
         3909 Halls Ferry Road
         Vicksburg, MS 39180-6199

2   Wright Lab Armament Directorate
         WL/MNSI
         Attn: Dave M. Belk
              Yen Tu
         101 W. Eglin Blvd., Ste 251
         Eglin AFB, FL 32542-6810

1	MS0439	D.B. Longcope, 9234
1	MS0303	M.J. Forrestal, 2411
1	MS0437	S.W. Attaway, 9118
1	MS0483	N.R. Hansen, 2165
1	MS0303	J.L. McDowell, 2411
1	MS0437	R.K. Thomas, 9118
1	MS0439	D.R. Martinez, 9234
1	MS0820	P. Yarrington, 9232
1	MS0303	J. Hickerson, 2411
1	MS0481	T. Hendrickson, 2105
1	MS0842	T. Hitchcock, 2521
20	MS0437	M.R. Tabbara, 9118

20 MS0303 T.L. Warren, 2411

1 MS0303 R. Lundgren, 2411

1 MS0419 J. Rogers, 5412

1 MS9042 E.P. Chen, 8742

1 MS0820 S. Silling, 9232

1 MS0437 J.D. Gruda, 9118

1 MS0437 K.E. Metzinger, 9118

1 MS0437 F.J. Mello, 9118

1 MS9018 Central Tech Files, 8940-2

5 MS0899 Technical Library, 4916

2 MS0619 Review & Approval Desk, 12690
For DOE/OSTI